Preclinical pharmacokinetic/pharmacodynamic models of gefitinib and the design of equivalent dosing regimens in EGFR wild-type and mutant tumor models

Shining Wang, Ping Guo, Xiaomin Wang, Qingyu Zhou, and James M. Gallo

Department of Pharmaceutical Sciences, School of Pharmacy, Temple University, Philadelphia, Pennsylvania

Abstract

Epidermal growth factor receptor (EGFR) inhibitors, such as gefitinib, are examples of targeted anticancer drugs whose drug sensitivity is related to gene mutations that adds a pharmacogenetic (PG) dimension to any pharmacokinetic (PK) and pharmacodynamic (PD) analysis. The goal of this investigation was to cast the combined PG/PK/PD variables into models that could be used to design equivalent PK/PD dosing regimens for gefitinib in genetically distinct tumor models. To this end, groups of mice bearing either s.c. LN229-wild-type EGFR or LN229-EGFRvIII mutant tumors, an EGFR inhibitor-sensitizing mutation, were given gefitinib at doses of 10 mg/kg i.v., 50 mg/kg intraarterially, and 150 mg/kg p.o. In each group, gefitinib plasma and tumor concentrations were quantitated, as were tumoral amounts of phosphorylated extracellular signal-regulated kinase (ERK) 1/2 (pERK), a PD end point that was shown to respond in a dose-dependent manner in each tumor type. Hybrid physiologically based PK/PD models were developed for each tumor type, which consisted of a forcing function describing the plasma drug concentration profile, a tumor compartment depicting drug disposition in tumor, and a mechanistic target-response PD model characterizing pERK in the tumor. Gefitinib showed analogous PK properties in each tumor type yet different PD characteristics consistent with the EGFR status of the tumors. Using the PK/PD model for each tumor type, simulations were done to define multiple-dose regimens for gefitinib that yielded equivalent PD profiles of pERK in each tumor type. The novel concept of PK/PD equivalent dosing regimens could be applied in drug development and to delineate PG differences in drug activity. [Mol Cancer Ther 2008;7(2):407–17]

Introduction

Anticancer drug development is an arduous process that encompasses drug discovery and development phases, in which the latter consists of a series of preclinical *in vitro* cell-based and *in vivo* animal investigations before entry into the clinic. A large portion of the *in vivo* animal studies is concerned with toxicity tests in various animal species, and additional tumor efficacy studies in rodents, whereby a reduction in the size of s.c. tumors is deemed the harbinger of anticancer efficacy. The reliance on tumor size is fraught with limitations because drug treatment regimens are chosen semi-empirically, and collection of pharmacokinetic (PK) and pharmacodynamic (PD) information is not a priority. In this approach, drugs that fail to show substantial reductions in tumor size may be discarded prematurely, and drug successes, those that appreciably shrink tumors, are moved into the clinic without an understanding of the PK and PD behavior of the drug in the tumor. This latter deficiency is remarkable in an age of targeted drugs whose signaling networks are vital to their mechanism of action and offer a rich PD milieu that could aid therapy. A goal of this investigation was to focus on drug disposition and dynamics in the tumor as a foundation to support alternate drug development paradigms.

To show certain aspects of our drug development approach, we chose gefitinib (Iressa, AstraZeneca), an epidermal growth factor receptor (EGFR) inhibitor that is undergoing clinical evaluation in numerous cancer types and is conditionally approved for the treatment of non–small cell lung cancer (1). The EGFR and a related family member, ErbB2, serve as cell surface drug targets, and the basis for a concerted drug development effort as their dysregulation contributes to the development and progression of several human cancers through uncontrolled cell proliferation, angiogenesis, and apoptosis inhibition (2, 3). Gefitinib is a low molecular weight (i.e., 446.9 Da) anilinoquinazoline, which is an p.o. active, selective EGFR tyrosine kinase inhibitor that competitively and reversibly binds to the ATP-binding sites of EGFR, causing downregulation of EGFR phosphorylation and subsequent downstream signaling molecules (4). A growing focus has been in identifying molecular determinants for EGFR inhibitor sensitivity that are often related to mutations in the *EGFR* gene (5) yet are not necessarily conserved among different cancer types. In glioblastoma, EGFR has been frequently found dysregulated, including protein overexpression, gene amplification, and *EGFR* gene mutations (6). EGFRvIII, the variant receptor with a truncated extracellular domain, is

doi:10.1158/1535-7163.MCT-07-2070

observed in 60% to 70% of EGFR-overexpressing glioblastomas (7). The absence of the extracellular ligand-binding domain results in the constitutive activation of the receptor and, in the presence of PTEN (phosphatase and tension homologue deleted in chromosome 10), can sensitize glioblastomas to EGFR inhibitors (8, 9). The availability of glioblastoma cell lines and tumor models that differ only in EGFR status (wild-type versus EGFRvIII) provided an opportunity to consider the pharmacogenetic basis of PK/PD models for gefitinib, which led to the concept of equivalent PK/PD dosing regimens, the latter providing a quantitative basis to account for PK and PD differences in drug response in different tumors. This new concept could have potential significance in the renovation of drug development paradigms and in the clinic to achieve an optimal dose response in individual patients.

Materials and Methods

Chemicals and Reagents

Gefitinib was kindly provided by AstraZeneca. LN229-EGFRvIII mutant cell line was a gift from Dr. W.K. Cavenee (University of California, San Diego, CA). LN229-wild-type EGFR cell line was purchased from the American Type Culture Collection. The following reagents were purchased: DMEM (Mediatech, Inc.); fetal bovine serum (Invitrogen); sulforhodamine B (Sigma-Aldrich Co.); anti-EGFR, anti–phosphorylated AKT, anti-AKT, and anti–extracellular signal-regulated kinase (ERK) antibodies (Santa Cruz Biotechnology); anti-PTEN and anti–phosphorylated ERK (pERK; Cell Signaling Technology); Matrigel matrix (Becton Dickinson); protein assay reagent (Bio-Rad); chemiluminescence detection system (Perkin-Elmer); and ELISA kit to measure pERK (R&D Systems). All other chemicals and reagents were obtained from commercial suppliers.

Cell Culture

Human glioblastoma cell lines LN229-wild-type EGFR and LN229-EGFRvIII mutant cells were cultured in DMEM supplemented with 10% heat-inactivated fetal bovine serum. Cells were grown under standard cell culture condition in humidified atmosphere with 5% CO_2 at 37°C.

Cytotoxicity Assay

The cytotoxicity of gefitinib to LN229-EGFR wild-type and LN229-EGFRvIII cells was determined using a colorimetric sulforhodamine B–based assay (10). Cell suspensions of 100 μL (2×10^3 cells) were seeded in 96-well plates and allowed to attach to the surface by overnight incubation. Afterwards, cells were treated with gefitinib at various concentrations for 72 h. At the end of the treatment, cells were fixed with 10% (v/v) trichloroacetic acid and stained with 0.4% sulforhodamine B. The optical densities were measured with a SpectraMax M2 microplate reader (Molecular Devices) at a wavelength of 570 nm. The IC_{50} values were defined as the drug concentration that was required to reduce the number of viable cells to 50% compared with control treatment (vehicle alone). Each IC_{50} mean value was obtained from six independent experiments.

Western Blot Assay

To examine protein expression levels, subconfluent tumor cells cultured in DMEM with 10% heat-inactivated fetal bovine serum were treated with different concentrations of gefitinib for 1 h. The cells were rinsed with ice-cold PBS and cell lysates were prepared in a cell lysis buffer containing 50 mmol/L Tris-HCl (pH 7.5), 137 mmol/L NaCl, 10% glycerol, 1% NP40, 2 mmol/L EDTA, 25 mmol/L β-glycerophosphate, 50 mmol/L NaF, 10 mmol/L sodium pyrophosphate, 1 mmol/L Na_3VO_4, and a protease inhibitor cocktail. Equal amounts of proteins (20 μg) were electrophoresed on precast SDS-polyacrylamide gels (Bio-Rad) and transferred to Immobilon membranes (Millipore). After transfer, membranes were blocked with 5% nonfat milk at room temperature for 1 h and subsequently probed with various primary antibodies overnight at 4°C. The blots were washed and then incubated with horseradish peroxidase–conjugated secondary antibodies (Santa Cruz Biotechnology) at room temperature for 1 h and visualized by an enhanced chemiluminescence system.

In vivo Experiments of Gefitinib in Xenografts of EGFR Wild-Type and Mutant Tumors

Male athymic Swiss mice (*nu/nu* genotype) weighing 20 to 25 g were supplied by Taconic Co. and maintained in the American Association for the Accreditation of Laboratory Animal Care–accredited University Laboratory Animal Resources of Temple University. All animal studies were approved by the Institutional Animal Care and Use Committee. LN229-wild-type EGFR or LN229-EGFRvIII mutant tumor cells were harvested *in vitro*, and 5×10^6 cells were suspended in a mixture of PBS and Matrigel in a total volume of 200 μL (PBS/Matrigel, 1:2). Afterwards, athymic mice were injected s.c. with the tumor cell suspensions in the dorsal neck region under anesthesia. Tumor diameter was measured with a vernier caliper (Fisher Scientific) and converted to tumor volumes using the formula $\pi/6 \times$ large diameter $\times$ (small diameter)^2 (11). For both LN229-wild-type EGFR and LN229-EGFRvIII mutant xenografts, when tumor size reached ~1.3 mL volume, athymic mice were assigned to different treatment groups: (*a*) 10 mg/kg gefitinib as an i.v. bolus through a tail vein, (*b*) 50 mg/kg gefitinib as an intraarterial (i.a.) infusion over 4 min through the carotid artery, and (*c*) 150 mg/kg gefitinib by p.o. gavage. For the 50 mg/kg i.a. administration group, the right carotid artery was surgically catheterized for drug administration the day before gefitinib treatment so all animals were conscious at the time of drug administration. Gefitinib was dissolved in DMSO and further diluted with 4.5% glucose (pH 4) to 3.5 mg/mL for i.v. and i.a. administrations or suspended in 1% polysorbate-80 to 10 mg/mL for p.o. administration. A serial sacrifice design was used with blood and tumor samples collected before dose and at 0.25, 0.5, 1, 2, 4, 6, 8, 12, 24, and 36 h following intravascular administrations and before dose and at 0.5, 1, 2, 3, 4, 6, 8, 12, 16, 24, and 36 h following p.o. administrations. At the scheduled sampling times, mice were briefly anesthetized with isoflurane, and terminal blood samples were collected

through the inferior vena cava followed by rapid tumor excision. Plasma, harvested from blood, and tumor samples were stored at −80°C until further analysis.

Drug Analysis

Gefitinib concentrations in plasma and tumor homogenate were measured by using an electrospray ionization liquid chromatography-tandem mass spectrometry system (Applied Biosystems) set in positive ion scan mode. Plasma samples of 10 μL each were deproteinized with 40 μL methanol containing an internal standard (*E*)-*N*-(3-amino-4-methoxyphenyl)-3-(2,4,6-trimethoxyphenyl)pro-2-enamide (ON27040) followed by centrifugation at 15,000 rpm for 5 min. To 40 μL of tumor homogenate [10% (w/w) tumor/water], 120 μL of methanol containing ON27040 were added followed by centrifugation at 15,000 rpm for 15 min. For both plasma and tumor samples, aliquots of 5 μL supernatant were injected into the liquid chromatography-tandem mass spectrometry system. The chromatographic separation system consisted of a guard cartridge (C18, 4.0 × 2.0 mm; Phenomenex), an analytic column (Luna C18, 3 μm particle size, 50 × 2.0 mm; Phenomenex), and a mobile phase of acetonitrile/10 mmol/L ammonium formate (65:35, v/v) at a flow rate of 0.2 mL/min. The column temperature was maintained at 40°C. The column effluent was monitored at the following precursor-product ion transitions: *m/z* 447.2→100.2 for gefitinib and *m/z* 359.1→220.9 for ON27040 with a dwell time of 400 ms for each ion transition. The retention time was 1.5 min for gefitinib and 1.4 min for ON27040. The lower limit of quantitation was 3.6 and 6.9 ng/mL for plasma and tumor homogenate, respectively. Linear calibration ranges of gefitinib were between 3.6 and 2,616 ng/mL in plasma and between 6.9 and 5,032 ng/mL in tumor homogenate. Both the accuracy and precision of the assay were <15% as expressed by intraday and interday percentage error.

pERK Analysis

The amounts of pERK in tumors were measured with an ELISA kit (R&D Systems) in which 50 mg of tumor samples were homogenized with a tumor lysis buffer containing 50 mmol/L Tris-HCl (pH 7.5), 137 mmol/L NaCl, 10% glycerol, 1% NP40, 2 mmol/L EDTA, 25 mmol/L β-glycerophosphate, 50 mmol/L NaF, 10 mmol/L sodium pyrophosphate, 1 mmol/L Na_3VO_4, 6 mol/L urea, and a protease inhibitor cocktail. After centrifugation (15,000 rpm, 15 min at 4°C) of the tumor lysate, the supernatant was collected and the protein concentration was determined by using the Bio-Rad protein assay reagent. ELISAs were done on flat-bottomed, 96-well polystyrene microplates (Corning), where each microtiter well was coated with 100 μL of the capture antibody (4 μg/mL in PBS) at room temperature overnight. The unbound capture antibody was removed with three washes with PBS containing 0.05% Tween 20. After 2 h of blocking with 1% bovine serum albumin in PBS and subsequent washing steps, 100 μL aliquots of tumor lysate with normalized protein concentration were added to each microtiter well for a 2-h incubation at room temperature. Following washing thrice with PBS containing 0.05% Tween 20, 100 μL of a biotinylated detection antibody

(7.2 μg/mL) were applied and incubated at room temperature for another 2 h. Subsequently, the plates were washed thrice and 100 μL of diluted streptavidin-horseradish peroxidase were added to each well for a 20-min incubation. Following a set of wash steps, 100 μL of substrate solution were applied to each well for 20 min and the reaction was stopped by adding 50 μL of 2 mol/L H_2SO_4 to each well. The absorbance was measured at 450 nm by using a SpectraMax M2 microplate reader. A seven-point standard curve was created by plotting the absorbance with respect to the corresponding concentration value in pg/mL. Afterwards, the pERK concentration in tumor lysate was determined based on their absorbance values. Each tumor pERK concentration value was obtained by averaging the quadruplicate measurements in two independent experiments and expressed as a fraction relative to the tumor pERK concentration in the predose sample.

PK and PD Analysis

PK and PD data analyses were conducted with the SAAMII software (version 1.2, University of Washington, Seattle, WA; ref. 12) based on a sequential modeling approach of first defining the PK model and then the PD model. A physiologically based hybrid PK model was simultaneously fit to all the observed plasma and tumor gefitinib concentrations obtained from each dose level. The hybrid PK model consisted of a two-compartment systemic model describing the plasma gefitinib concentration profile and a single tumor compartment characterizing gefitinib concentrations in tumor. Variables estimated from the hybrid PK model included the elimination rate constant (K_{10}), volume of distribution of the central compartment (V_c), absorption rate constant (K_a), bioavailability (F), intercompartmental rate constants (K_{12} and K_{21}), and physiologic variables including the tumor blood flow rate (Q) and tumor to plasma partition coefficient (R_i). The mean value of the actual tumor volume measured on the day of the PK study was applied as the volume of tumor compartment (V_t). Once the hybrid PK model was finalized, the associated PK variables were set as constant and linked to the PD model.

The fractional inhibition of pERK in tumor after gefitinib administrations was used as the PD response and determined as the measured pERK concentration in each tumor sample divided by the predose pERK concentration in tumors. The PD models consisted of a two-compartment target-response model composed of a target compartment representing phosphorylated EGFR (pEGFR) and a response compartment representing pERK. The rate equations are provided below in which it can be seen that an inhibitory E_{max} model is used to link the PK model, in terms of the gefitinib concentration in tumor (C_t), to the PD model:

$$\frac{d\text{pEGFR}}{dt} = K_{in} \cdot \left(\text{pEGFR}^0 - \frac{I_{max} \cdot C_t}{IC_{50} + C_t}\right) - K_{tr} \cdot \text{pEGFR}$$

$$\frac{d\text{pERK}}{dt} = K_{tr} \cdot \text{pEGFR} - K_{out} \cdot \text{pERK}$$
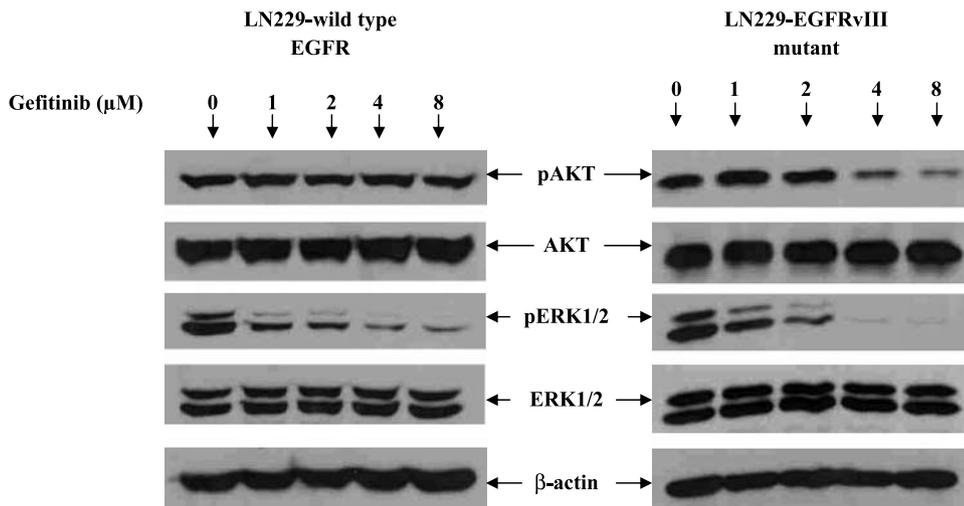
Figure 1. Effect of gefitinib on the phosphorylation of AKT and ERK in the pair of EGFR wild-type and mutant cell lines as a function of drug concentration. LN229-wild-type EGFR and LN229-EGFRvIII cells cultured in DMEM with 10% heat-inactivated fetal bovine serum were treated with gefitinib at the indicated concentrations for 1 h. A total of 20 μg protein extracts were subjected to SDS-PAGE and Western blots were done subsequently to measure the protein expression levels, including phosphorylated AKT (pAKT), total AKT, pERK, total ERK, and β-actin.

where K_{in} is the zero-order rate constant for the formation of pEGFR, K_{tr} is the first-order rate constant depicting the signal transduction pathway from the drug target compartment (pEGFR) to the response compartment (pERK), and K_{out} is the first-order rate constant representing degradation and dephosphorylation of pERK. $pEGFR^0$ was the baseline tumor pEGFR level and I_{max} was the maximum inhibitory response of pEGFR, which were both set equal to 1. Other model variables were defined as follows: C_t is the gefitinib concentration in tumor and IC_{50} is the gefitinib tumor concentration corresponding to 50% of I_{max}. The two-compartment target-response model was individually fitted to the fractional pERK measurements obtained following 10 mg/kg i.v., 50 mg/kg i.a., and 150 mg/kg p.o. single-dose administrations for each tumor type. The final variables to be estimated were IC_{50}, K_{in}, K_{tr}, and K_{out}.

The best-fit hybrid PK/PD models were evaluated according to the statistical criteria from SAAM II program, including the minimization of the objective function, the Akaike information criteria, and the precision of variable estimation as measured by the coefficient variances. The fractional SD error models were used in fitting both the PK and PD models.

Results

In vitro Investigations of Gefitinib in EGFR Wild-Type and Mutant Glioblastoma Cell Lines

Both clinical and preclinical studies have shown that the coexpression of EGFRvIII mutant and PTEN in glioblastoma cells served as molecular determinant for enhanced response to EGFR inhibitors (8, 9). We confirmed these findings in the LN229 cells by Western blot analyses (see Supplementary Fig. S1).[1] PTEN at 54 kDa was identified in both of the cell lines, whereas a 170-kDa wild-type EGFR

and a 140-kDa EGFRvIII mutant were detected in LN229-wild-type EGFR and LN229-EGFRvIII mutant cell lines, respectively. These expression patterns indicated that these two cell lines offered a pharmacogenetic basis to contrast PD differences due to gefitinib.

Before the PK/PD investigations in tumor-bearing mice, *in vitro* studies were completed in the two cell lines to confirm the likely differences in sensitivity to gefitinib and to identify PD markers that could subsequently serve as putative PD end points in tumor-bearing animals. The cytotoxicity studies showed that gefitinib was more active in LN229-EGFRvIII cells [i.e., IC_{50} = 4.3 (mean) ± 1.6 (SD) μmol/L; n = 6] than in LN229-wild-type EGFR cells [i.e., IC_{50} = 8.5 (mean) ± 1.3 (SD) μmol/L; n = 6], a result consistent with the different responsiveness of glioblastomas to gefitinib previously reported (8), and suggested that PD end points would also respond differently to gefitinib.

As a tyrosine kinase inhibitor, gefitinib down-regulates tyrosine kinase−induced EGFR phosphorylation and subsequently inhibits downstream signal transduction proteins (3). Based on pertinent signal transduction pathways, the effect of gefitinib on several likely PD end points, including AKT, ERK, p38 mitogen-activated protein kinase, signal transducers and activators of transcription 3, and c-Fos, was examined in the pair of EGFR wild-type and mutant cell lines as a function of gefitinib concentrations. Western blot analysis showed that pERK was inhibited in a dose-dependent manner in both cell lines, whereas phosphorylated AKT showed a dose-dependent inhibition only in LN229-EGFRvIII mutant cells (see Fig. 1). The other candidate PD end points, including p38 mitogen-activated protein kinase, signal transducers and activators of transcription 3, and c-Fos, did not display apparent dose-dependent inactivation following gefitinib treatment. The most remarkable finding in this set of *in vitro* studies was that pERK might serve as a common PD end point for both tumor types *in vivo*, which would facilitate the development of contrasting PD models and the design of PK/PD equivalent dosing regimens.

---

[1] Supplementary material for this article is available at Molecular Cancer Therapeutics Online (http://mct.aacrjournals.org/).

Table 1. PK model variables of gefitinib in plasma and tumor from LN229-wild-type EGFR and LN229-EGFRvIII mutant tumor-bearing athymic mice following 10 mg/kg i.v., 50 mg/kg i.a., or 150 mg/kg p.o. single-dose administrations

Variables	LN229-wild-type EGFR tumor-bearing group	LN229-EGFRvIII mutant tumor-bearing group
F	0.45 (6.9)*	0.52 (6.6)
K_{10} (h^{-1})	0.85 (17.8)	0.70 (12.5)
K_{12} (h^{-1})	1.57 (21.6)	0.93 (20.0)
K_{21} (h^{-1})	0.41 (12.1)	0.37 (11.4)
K_a (h^{-1})	0.88 (14.6)	0.82 (13.6)
Q (mL·h^{-1})	4.5 (13.5)	4.4 (10.8)
R_I	8.2 (7.3)	9.8 (6.7)
V_c (mL)	75.0 (19.5)	103.8 (14.0)
V_t (mL)	1.3	1.3

*Values represent mean (% coefficient of variation) of model fitted variables.

PK/PD Models of Gefitinib in Wild-Type and vIII Mutant EGFR Tumors

The development of preclinical hybrid PK/PD models of anticancer drugs requires extensive measurements of drug concentrations in plasma and tumor, and the associated PD end points to ensure that the most salient features of drug disposition and dynamics are characterized. Therefore, a series of dose-dependent investigations of gefitinib in both LN229-wild-type EGFR and LN229-EGFRvIII mutant tumor-bearing mice were done, which consisted of a PK phase for the measurement of plasma and tumor drug concentrations and a PD phase for the quantitation of tumor pERK. The dose range of gefitinib of 10 mg/kg i.v. to 150 mg/kg p.o., about a 7-fold dose difference based on the systemic bioavailability of gefitinib (see Table 1), permitted an assessment of whether gefitinib possessed linear or nonlinear PK properties as well as an estimate of its systemic bioavailability, which was needed to simulate the PK/PD behavior of gefitinib following relevant multiple-dose p.o. treatments.

Hybrid physiologically based PK/PD models (see Fig. 2) were used to describe the accumulated PK/PD data from the three different dosing regimens. It was felt that these models offered the best opportunity to capture the PK/PD characteristics of gefitinib in the tumor and retain many physiologic features, such as blood flow and tumor volumes in the target tissue, which would provide a robust modeling tool that could be modified in a species scale-up procedure (13, 14). The hybrid PK/PD models were developed in a sequential manner with the definition of the PK model followed by the PD model. By fitting the PK models simultaneously to the combined gefitinib concentrations from all treatments, a single PK model for each tumor type was obtained. The best-fit PK models consisted
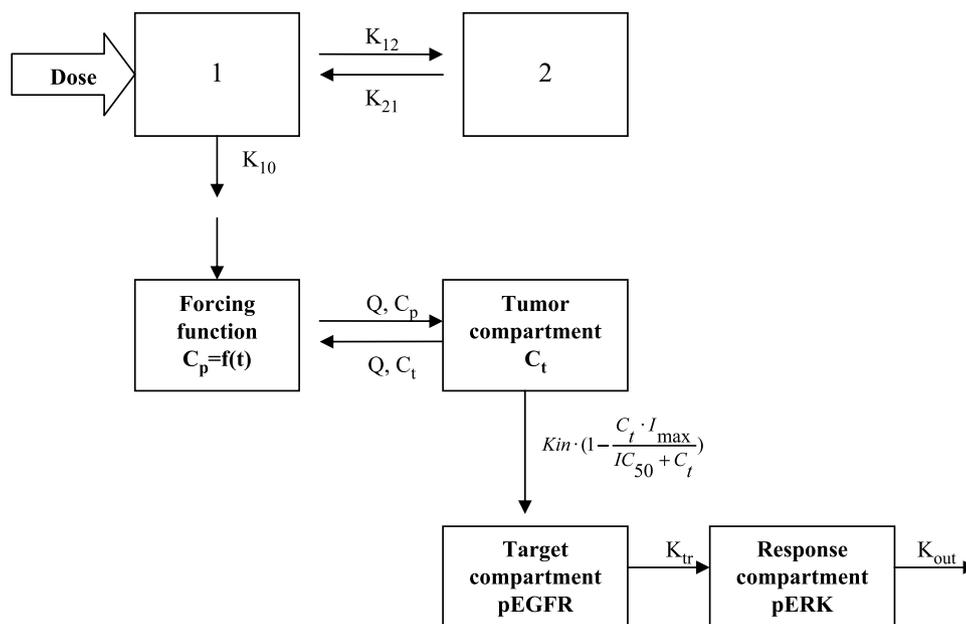

Figure 2. Schematic representation of a hybrid PK/PD model consisting of a two-compartment systemic disposition model, a one-compartment tumor model, and a two-compartment target-response model. The model was developed by a sequential method in which the PK model was initially defined and then followed by definition of the PD model. The PK model variables included the elimination rate constant (K_{10}), volume of distribution in the plasma compartment (V_c), intercompartment transfer rate constants (K_{12} and K_{21}), absorption rate constant (K_a), bioavailability (F), blood flow rate (Q), and tumor to plasma partition coefficient (R_i). The tumor volume (V_t) was fixed to the actual mean tumor volume on the day of PK study. The PD model variables included tumor drug concentration for 50% inhibition of pEGFR (IC_{50}), the zero-order rate constant for the formation of pEGFR (K_{in}), the rate constant from the drug target compartment (pEGFR) to the response compartment (pERK; K_{tr}), and a first-order rate constant for degradation and dephosphorylation of pERK (K_{out}). The pEGFR^0 and I_{max} were fixed as 1. This hybrid PK/PD model was identified as the best-fit model to depict gefitinib PK/PD characteristics in LN229-wild-type EGFR or LN229-EGFRvIII mutant tumor-bearing mice.
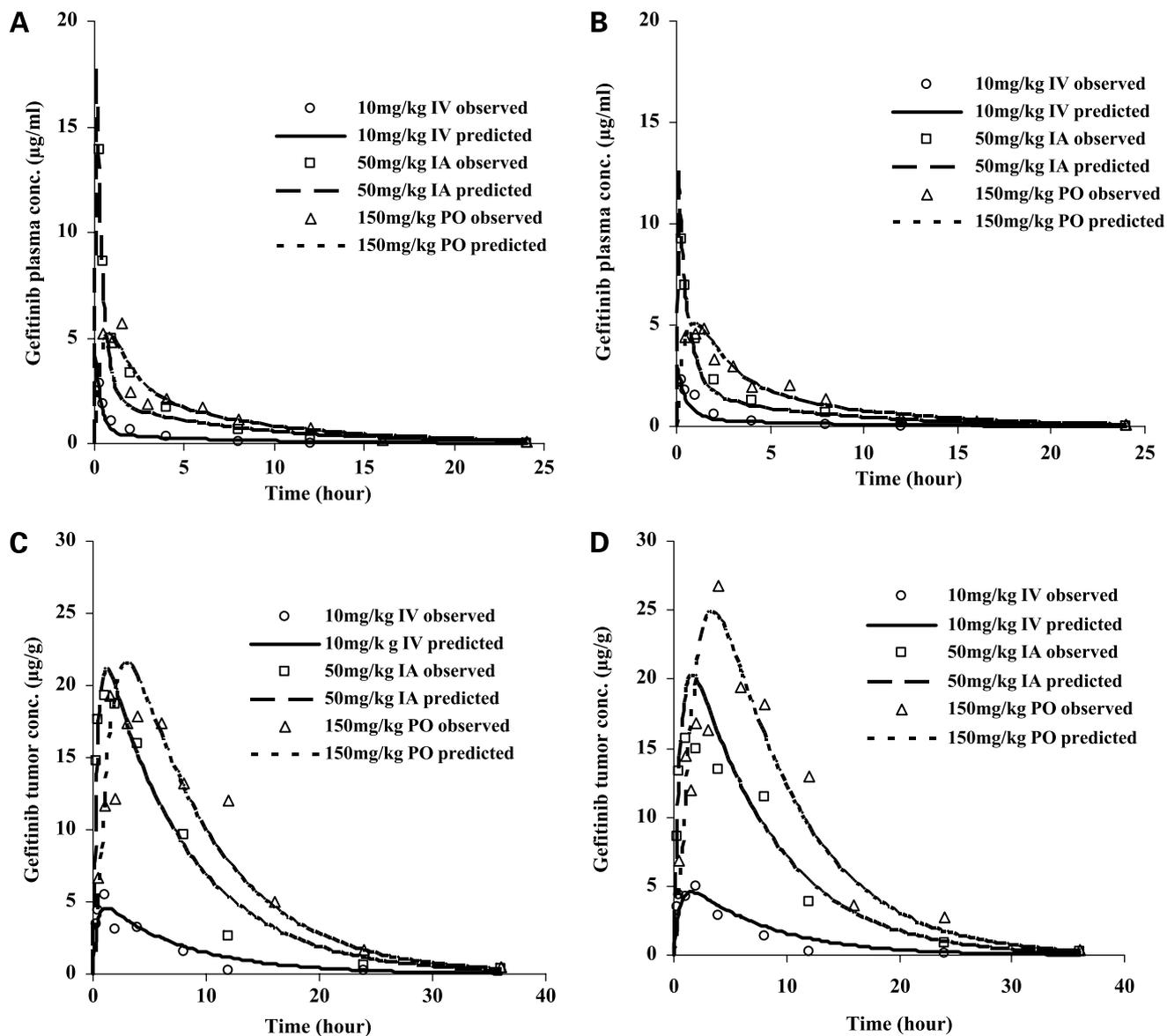
Figure 3. PK modeling of gefitinib in LN229-wild-type EGFR (**A** and **C**) or LN229-EGFRvIII mutant (**B** and **D**) tumor-bearing mice following 10 mg/kg i.v., 50 mg/kg i.a., or 150 mg/kg p.o. single-dose administrations. For either LN229-wild-type EGFR or LN229-EGFRvIII mutant tumor-bearing group, a hybrid PK model, consisting of a forcing function to describe the plasma gefitinib concentration profile and a tumor compartment to represent gefitinib disposition in tumor tissue, was fit to the combined PK data simultaneously. The model predicted (——, 10 mg/kg i.v.;– –, 50 mg/kg i.a.; ---, 150 mg/kg p.o.) and mean (*n* = 3 – 4) observed (O, 10 mg/kg i.v.; □, 150 mg/kg i.a.; Δ, 150 mg/kg p.o.) gefitinib concentrations are presented for plasma (**A**) and tumor (**C**) of LN229-wild-type EGFR tumor-bearing group and plasma (**B**) and tumor (**D**) of LN229-EGFRvIII mutant group, respectively.

of a two-compartment systemic model that defined the forcing function input into a single tumor compartment model. Generally, the predicted plasma and tumor concentration profiles agreed with the observed values, although there were slight underestimations or overestimations that occurred at several time points for either plasma or tumor drug concentrations (see Fig. 3) yet in a random manner. Moreover, given the fairly analogous observed gefitinib concentration-time profiles for the wild-type and mutant EGFR groups, it was not surprising to see similar values for

many of the PK variables in these tumor groups (see Table 1). The bioavailability was estimated as 0.45 in wild-type group and 0.52 in mutant group, and the systemic drug clearance ($V_c \times K_{10}$) was calculated as 63.8 mL/h and 72.7 mL/h for the two tumor groups, respectively. In fact, there were no significant differences in the PK variables between the two tumor groups except in the intercompartmental rate constant $K_{(1, 2)}$. In the tumor compartment, the blood flow rate (Q) was estimated as 4.5 mL/min for wild-type group and 4.4 mL/min for vIII mutant group, which

agreed with values directly measured in mouse tumors (15, 16). For each tumor group, the estimated gefitinib tumor to plasma partition coefficient (R_i) was much greater than 1 and ranged from 8 to 9, attesting to the ability of gefitinib to enter tumors, at least those in which there is not an intact anatomic barrier, such as the blood-brain barrier.

Once the hybrid PK model for each EGFR wild-type and mutant xenograft was established, the PK model and associated variables were linked to candidate PD models representing the inhibition of pERK in tumors. This sequential PK/PD modeling strategy greatly minimized model identification problems and facilitated more accurate model variables and predictions compared with attempts to fit both the PK and PD models simultaneously. Given the previously defined PK models for the two tumor types, candidate PD models that were applied to the pERK measurements included simple direct and indirect response models (17, 18) and a three-compartment target-response model containing an intermediate signaling compartment between pEGFR and pERK. Ultimately, the best-fit PD model to describe the inhibition of ERK phosphorylation was a two-compartment target-response model, in which the target compartment represented pEGFR and the response compartment represented pERK. It was found that individual fitting of the PD models to pERK data from each dose best captured the PD profiles (see Fig. 4) unlike the simultaneous fits of the PK models. Generally, the pERK profiles consisted of a relatively rapid decline and near baseline return over 24 to 36 h. In both tumor groups, higher gefitinib doses of 50 mg/kg i.a. or 150 mg/kg p.o. produced more profound nadirs than 10 mg/kg i.v., with the observed nadir values over all dose levels ranging from 0.14 to 0.53 in wild-type tumors and from 0.03 to 0.38 in vIII mutant tumors, respectively, which suggested a pharmacogenetic-based, dose-dependent phenomenon. The baseline $pEGFR^0$ and I_{max} were set equal to 1 based on the assumption that the phosphorylation of pEGFR was not inhibited in the absence of gefitinib and
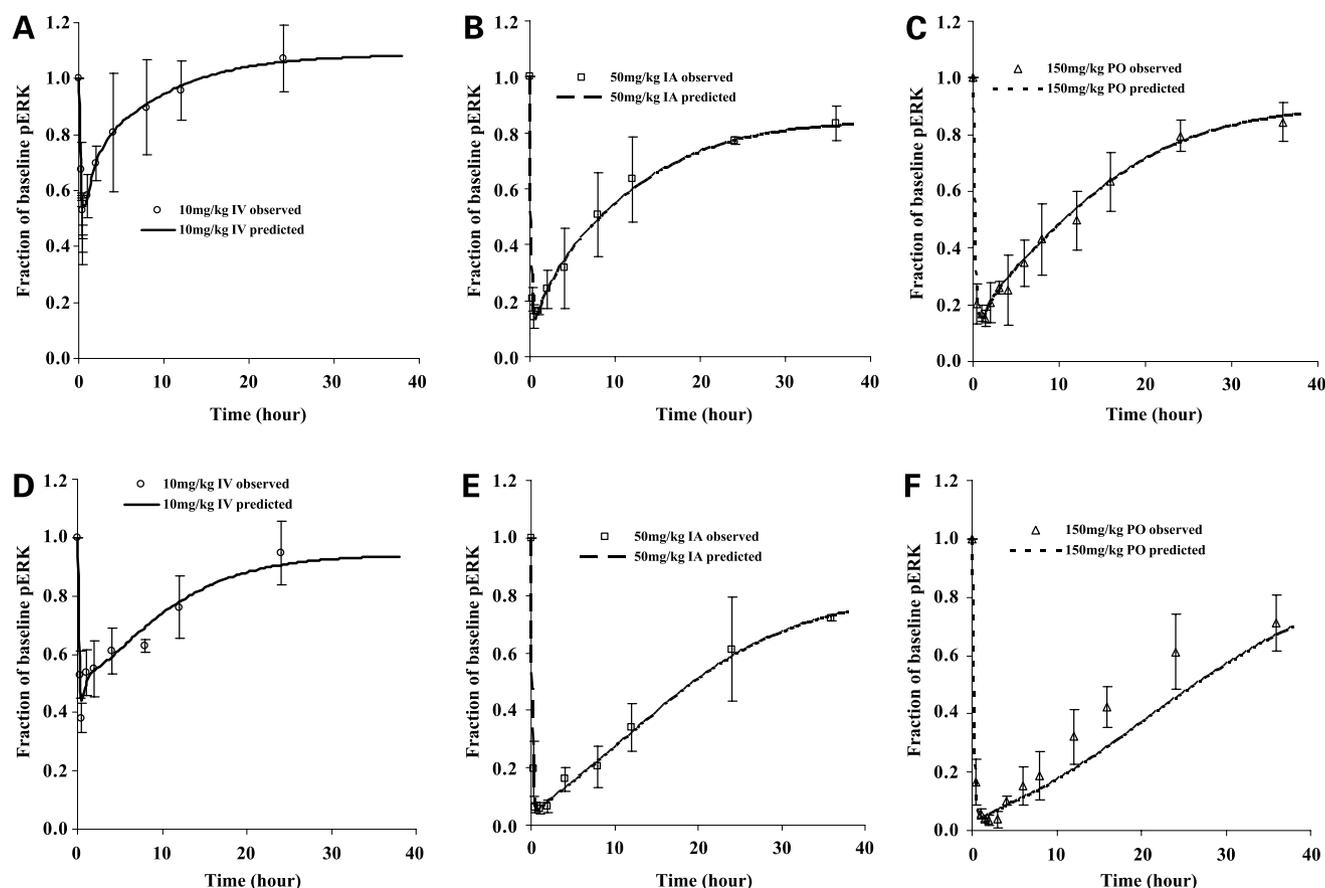

Figure 4. PD modeling of gefitinib in LN229-wild-type EGFR (**A – C**) or LN229-EGFRvIII mutant tumors (**D – F**) following 10 mg/kg i.v., 50 mg/kg i.a., or 150 mg/kg p.o. single-dose administrations. Once the PK model for each tumor group was developed, the model variables were linked to a PD model characterizing the inhibition of pERK. A two-compartment target-response model, consisting of a drug target compartment representing the inhibition of pEGFR and a drug response compartment depicting the inhibition of pERK as measured biomarker, was individually fit to the PD data obtained from different dosing levels. The model predicted (——, 10 mg/kg i.v.; — —, 50 mg/kg i.a.; ---, 150 mg/kg p.o.) and observed (O, 10 mg/kg i.v.; □, 150 mg/kg i.a.; Δ, 150 mg/kg p.o.) fractional inhibition of pERK are presented for 10 mg/kg i.v. (**A**), 50 mg/kg i.a. (**B**), and 150 mg/kg p.o. (**C**) of wild-type tumor group and 10 mg/kg i.v. (**D**), 50 mg/kg i.a. (**E**), and 150 mg/kg p.o. (**F**) of vIII mutant tumor group, respectively. *Points*, mean; *bars*, SD.

that it could be fully inactivated at sufficiently high gefitinib tumor drug concentrations, respectively. Other model estimated variables are listed in Table 2. The IC_{50} values were found to be dose-dependent within each tumor group characterized by an increasing trend corresponding to increased tumor gefitinib area under the curve (AUC_t) values. There was an approximate 1.6- to 1.8-fold decrease in IC_{50} values for the vIII tumor group compared with the wild-type, consistent with the pharmacogenetic-based difference in gefitinib sensitivity and further agreed with their *in vitro* cytotoxicity difference. K_{tr}, a variable reflecting the signaling efficiency from pEGFR to pERK, showed an inverse relationship with gefitinib tumor concentrations, consistent with reduced signal transduction efficiency at higher AUC_t values. Moreover, given the correlation between IC_{50} and K_{tr} values to gefitinib AUC_t values in both tumor groups, functional relationships were defined (see Supplementary Fig. S2) and used in the equivalent PK/PD dosing simulations. The other PD variables (i.e., K_{in} and K_{out}) did not show a clear pattern or difference between dose levels or tumor types and displayed similar mean values of 4.53 h^{-1} versus 5.3 h^{-1} for K_{in} and 4.97 h^{-1} versus 5.67 h^{-1} for K_{out} in the wild-type and mutant EGFR tumor groups, respectively.

The Design of PK/PD Equivalent Dosing Regimens for EGFR Wild-Type and Mutant Tumors by Hybrid PK/PD Modeling

The final goal of the study was to use the PK/PD models for the wild-type and mutant EGFR tumors to define equivalent PK/PD dosing regimens. To mimic the dosing strategy of gefitinib in clinical studies, the simulation exercises used multiple-dose p.o. gefitinib administrations as input into the respective PK/PD models to determine which dose level yielded equivalent profiles of pERK. Given the similar PK properties in each tumor type and the greater sensitivity of the mutant EGFR tumor to inhibition of pERK, it was deduced that lower gefitinib doses would be needed in the mutant tumor group to obtain an equivalent PD profile as that in the wild-type group. The alternate strategy of increasing the dose level in the wild-type EGFR group was ruled out as the doses of gefitinib would likely be toxic (19). The simulation process was conducted in a sequential manner, initially using the PK model to generate the AUC_t values for each selected dose

regimen, which subsequently defined the PD variables (IC_{50} and K_{tr}) via the functional equations (see Supplementary Fig. S2), and the pERK profile using the target-response models. Because neither K_{in} nor K_{out} showed a dose dependence in either tumor group, their mean values from the three dose administrations were applied throughout the simulation process. Through a series of simulations, it was found that gefitinib doses of 150 mg/kg daily × 15 days and 70 mg/kg daily × 15 days generated an equivalent pERK profile in wild-type EGFR and EGFRvIII mutant tumor groups, respectively (see Fig. 5). It can be seen that the pERK curves for the two tumor groups essentially overlap; however, an additional quantitative criteria of the area between the effect curve, which has been used to describe drug-induced myelosuppression and other inhibitory PD models (20, 21), also established the equivalent nature of pERK inhibition with area between the effect curve values of 170.4 (fraction of pERK inhibition × day) for the wild-type EGFR tumor group and 168.5 for EGFRvIII mutant tumor group. The 2.1-fold greater daily dose in the wild-type EGFR tumor group yielded AUC_t in the wild-type tumor group ~1.8-fold greater than in the EGFRvIII mutant tumor group and of course was required to obtain the equivalent PD response and thus compensate for the lower sensitivity.

Discussion

Preclinical animal studies in the current anticancer drug development paradigm emphasize the use of rodent efficacy studies (22) and forgo the use of detailed PK and PD studies. Such PK/PD investigations provide an assessment of drug uptake into the tumor and enable PD end points to be measured at the target site, which is of increasing importance as targeted therapies are developed. Given the complexities of drug transport due to membrane transporters and the myriad of signaling pathways that may be altered, focusing PK/PD studies on the tumor should be of great value not only as a means to determine which targeted drug possesses the most favorable properties but also as a means to devise clinical dosing strategies. Thus, an important facet of the current investigation was to show the utility of a PK/PD tumor-directed approach to contrast the PK and PD characteristics of gefitinib, a model

Table 2. PD model variables of gefitinib corresponding to pERK inhibition in LN229-wild-type EGFR and LN229-EGFRvIII mutant tumors following 10 mg/kg i.v., 50 mg/kg i.a., or 150 mg/kg p.o. single-dose administrations

Variables	LN229-wild-type EGFR tumor			LN229-EGFRvIII mutant tumor		
	10 mg/kg i.v.	50 mg/kg i.a.	150 mg/kg p.o.	10 mg/kg i.v.	50 mg/kg i.a.	150 mg/kg p.o.
IC_{50} (µg/g)	12.1 (42.6)*	20.1 (33.8)	27.5 (31.4)	6.8 (26.8)	11.4 (23.6)	17.3 (16.9)
K_{in} (h^{-1})	3.6 (18.9)	6.6 (8.9)	3.4 (13.8)	5.1 (18.9)	5.7 (13.3)	5.1 (15.6)
K_{out} (h^{-1})	3.3 (16.7)	7.8 (7.8)	3.8 (12.8)	5.4 (17.2)	7.1 (7.0)	4.5 (14.5)
K_{tr} (h^{-1})	0.92 (20.5)	0.34 (12.0)	0.17 (11.2)	1.18 (18.8)	0.12 (19.7)	0.037 (21.9)

*Values represent mean (% coefficient of variation) of model fitted variables.

Figure 5. Equivalent PK/PD dosing. Model simulations of tumor gefitinib concentration-time profiles (**A**) and corresponding tumor pERK inhibition-time profiles (**B**) following 150 mg/kg p.o. daily × 15 d in LN229-wild-type EGFR tumor-bearing mice and 70 mg/kg p.o. daily × 15 d in LN229-EGFRvIII mutant tumor-bearing mice.
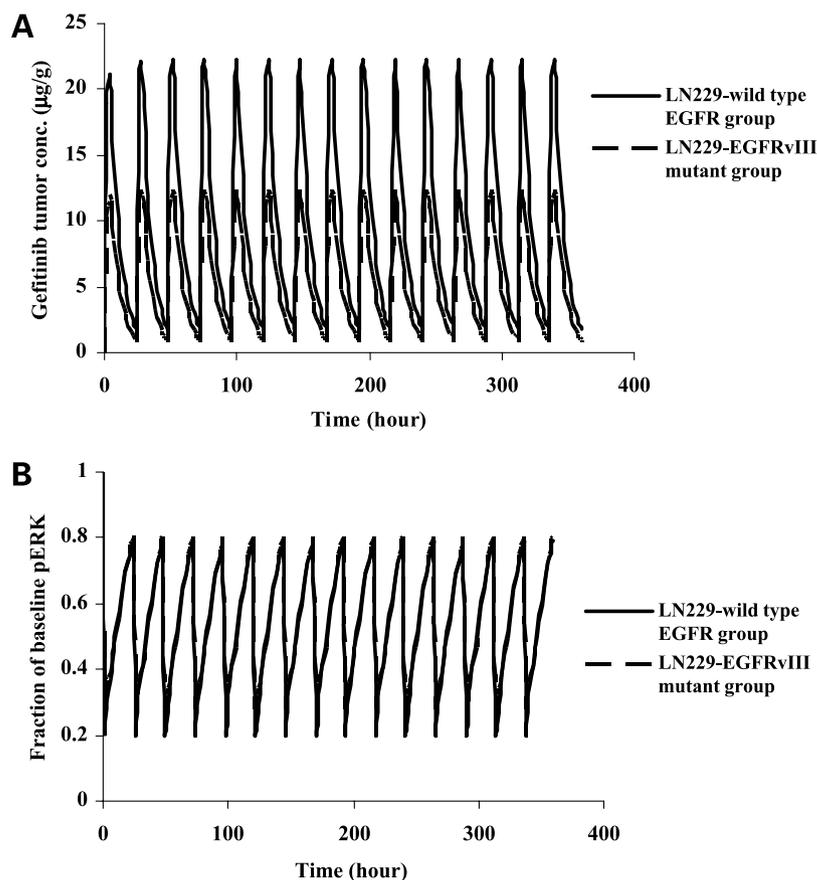
EGFR inhibitor, and then using the associated PK/PD models to introduce the concept of equivalent PK/PD dosing.

Before the *in vivo* xenograft studies, *in vitro* cytotoxicity and PD biomarker (see Fig. 1) studies were conducted to contrast the response of LN229-wild-type EGFR and LN229-EGFRvIII mutant cells to gefitinib. The 2-fold difference in cytotoxicity was anticipated; however, the search for a distinguishing PD end point was more involved due to the molecular mechanisms of gefitinib, which not only involves the unknown functions of proteins that might contribute to gefitinib sensitivity or resistance but also results from the intrinsic variance of different tumor cell lines (23–27). The net result of the *in vitro* studies indicated that pERK responded to gefitinib in a distinguishing and dose-dependent manner in the two glioma cell lines and thus might serve the same function *in vivo*.

To derive a tumor-based PK/PD model for gefitinib, we used three different doses and a serial sacrifice study design. An alternative serial blood and tumor microdialysis study design, as we have used previously (14, 28), was ruled out due to the poor dialyzability of gefitinib and the need to obtain a sufficient tumor mass for both drug and PD measurements. The PK characteristics of gefitinib in both the LN229-wild-type EGFR and LN229-EGFRvIII

mutant groups were quite similar (see Fig. 3 and Table 1) and anticipated, as the EGFR status was not considered to be a determinant of drug disposition, at least not at the scale of measuring gefitinib concentrations in tumor homogenate. The tumoral pERK measurements bore out the *in vitro* results with different pERK profiles observed in the two tumor types at equal gefitinib exposures (see Fig. 4). The physiologically based hybrid PK model of gefitinib consisted of a two-compartment systemic model and a one-compartment tumor model. The lumped one-compartment tumor models, one for wild-type and one for mutant EGFR tumors, are referred to as a blood flow–limited model and indicated that drug uptake is rapid and not limited by membrane transport across the vascular and tumor cell membranes. The physiologic representation of the tumor was considered advantageous on two accounts. One, future studies in this animal model that use a multiple-dose regimen could make use of the current variable set to ultimately derive a final model that could be linked to tumor size measurements and validate the equivalent PK/PD dosing protocols suggested here. Two, the physiologic representation could assist in a scale-up procedure to humans in which human values for tumor blood flow and volume could be substituted for the mouse values used here; however, additional studies in an orthotopic tumor model will be advantageous to scale up tumor/plasma

partition coefficient and membrane transport variables for gefitinib in human brain tumors.

As stated earlier, most preclinical PK studies focus on plasma drug concentration measurements, which may subsequently be linked to PD responses. In one example, a preclinical study of cetuximab established a PK/PD model between plasma drug concentration and the corresponding tumor PD response, in this case pEGFR (29). We chose to link the PK and PD components of our models by gefitinib tumor concentrations as this should be more indicative of drug concentrations at the target site, the EGFR located on the surface of tumor cells. The interaction between gefitinib concentrations at the target site or EGFR and pERK as the PD end point suggested the use of target-response PD model structure. This two-compartment PD model structure is generally similar to precursor-response drug tolerance models (30) and closely aligned to signal transduction models using a series of transfer compartments (18) and not dissimilar to a cellular PD model that accounted for general enzyme kinase and phosphatase activities (31). In the development of our target-response model, inclusion of a specific dephosphorylation reaction for pEGFR in the target compartment was found to be redundant and thus eliminated from the final model. Given that EGFR and ERK are not in direct signaling succession, an intermediate signaling compartment between the target-response sequence was considered; however, no improvement in model fitting resulted. It may be possible to expand the current PD model if other proteins in the signaling cascade are also measured in the tumor.

Unlike the PK model, whereby the hybrid physiologic model was simultaneously fit to gefitinib concentrations at each dose level, the PD model was best implemented by applying the PD model to pERK observations at each dose level. As can be seen from Table 2, IC_{50} and K_{tr} values exhibited a dose-dependent change for each tumor type, suggesting a nonlinear phenomenon. Such a change has been observed for EC_{50} variables, a component in an E_{max} model, which could not be explained mechanistically or cast into a convenient nonlinear model (17). We also did not find a suitable nonlinear PD model for gefitinib but did find functional relationships between both IC_{50} and K_{tr} and the AUC_t (see Supplementary Fig. S2) that was instrumental to define the equivalent PK/PD dosing regimens for the simulations because for each dose and AUC_t a different IC_{50} and K_{tr} value is defined. This potential dose-dependent behavior suggests the involvement of more complex molecular mechanisms related to gefitinib treatment, with the increased IC_{50} values possibly attributed to drug resistance, whereas the corresponding decreased K_{tr} implies an enhanced signaling efficiency downstream from EGFR and upstream from ERK. Additional mechanistic PK/PD investigations will be required to further interpret these PD model properties. Nonetheless, at this time, it is believed that the two-compartment inhibitory target-response model captured the essential features of the pERK profiles.

Equivalent PK/PD dosing is a simulation technique to devise analogous PK or PD profiles in the tumor or most relevant target site for drug action. For gefitinib, we used the PK/PD models for wild-type and mutant EGFR tumors to predict which p.o. multiple-dose regimens provided analogous PD profiles, in this case inhibition of pERK in tumors. As more targeted anticancer drugs are developed, the most relevant PD end points for drug activity will be sought and implementation of an equivalent PK/PD strategy might be advantageous. In the broader context of drug development, an equivalent PK/PD dosing strategy could be applied to a class of analogues to better define PK and PD differences. For example, an analogue requiring a 3-fold increase in the dose compared with the favored lead compound to achieve the same PD profile might be viewed as too toxic, whereas another analogue with a 1.5-fold dose enhancement might be acceptable and possibly preferred for development depending on its other attributes. In the absence of an equivalent PK/PD methodology, drugs possessing the best overall characteristics could be discarded prematurely because an optimal dosing regimen may not have been used in tumor size–based efficacy studies. The application of the equivalent PK/PD dosing strategy to wild-type and mutant tumors, as used in this investigation, could be broadened to other genetically defined tumors that affect drug activity, such as in the case of non–small cell lung cancer harboring L858R-sensitizing mutation in gefitinib treatment (25), and thus provide a quantitative picture of how likely drug activity will be found in a range of tumors. In either of these applications, an additional link between the PD end point, predicted from the PK/PD model, and antitumor efficacy could provide a final and definitive assessment of drug activity. This link could be defined with an extension of the PK/PD model to a tumor growth model that could be built from conventional tumor efficacy studies (32). In this scenario, a finding that inhibition of pERK correlated to tumor size could be used to replace extensive tumor size–based efficacy studies with PD end points to assess drug efficacy.

In summary, by using gefitinib as a model EGFR inhibitor and a pair of EGFR wild-type and mutant glioblastomas, comprehensive preclinical PK/PD investigations were conducted, which allowed the development of hybrid PK/PD models for each tumor type. The hybrid physiologically based PK/PD models were used as a simulation tool to design PK/PD equivalent dosing regimens, a new concept in cancer chemotherapy.

References

1. Kris MG, Natale RB, Herbst RS, et al. Efficacy of gefitinib, an inhibitor of the epidermal growth factor receptor tyrosine kinase, in symptomatic patients with non-small cell lung cancer: a randomized trial. JAMA 2003; 290:2149–58.

2. Janmaat ML, Giaccone G. Small-molecule epidermal growth factor receptor tyrosine kinase inhibitors. Oncologist 2003;8:576–86.

3. El-Rayes BF, LoRusso PM. Targeting the epidermal growth factor receptor. Br J Cancer 2004;91:418–24.

4. Wakeling AE, Guy SP, Woodburn JR, et al. ZD1839 (Iressa): an orally active inhibitor of epidermal growth factor signaling with potential for cancer therapy. Cancer Res 2002;62:5749–54.

5. Lynch TJ, Bell DW, Sordella R, et al. Activation mutations in the

epidermal growth factor receptor underlying responsiveness of non-small-cell lung cancer to gefitinib. N Engl J Med 2004;350:2129–39.

6. Lassman AB, Rossi MR, Razier JR, et al. Molecular study of malignant gliomas treated with epidermal growth factor receptor inhibitors: tissue analysis from North American Brain Tumor Consortium Trials 01-03 and 00-01. Clin Cancer Res 2005;11:7841–50.

7. Marie Y, Carpentier AF, Omuro AMP, et al. EGFR tyrosine kinase domain mutations in human gliomas. Neurology 2005;64:1444–5.

8. Mellinghoff IK, Wang MY, Vivanco I, et al. Molecular determinants of the response of glioblastomas to EGFR kinase inhibitors. N Engl J Med 2005;353:2012–24.

9. Sarkaria JN, Yang L, Grogan PT, et al. Identification of molecular characteristics correlated with glioblastoma sensitivity to EGFR kinase inhibition through use of an intracranial xenograft test panel. Mol Cancer Ther 2007;6:1167–74.

10. Skehan P, Storeng R, Scudiero D, et al. New colorimetric cytotoxicity assay for anticancer-drug screening. J Natl Cancer Inst 1990;82:1107–12.

11. Ciardiello F, Caputo R, Bianco R, et al. Antitumor effect and potentiation of cytotoxic drugs activity in human cancer cells by ZD1839 (Iressa), an epidermal growth factor receptor selective tyrosine kinase inhibitor. Clin Cancer Res 2000;6:2053–63.

12. Barrett PH, Bell BM, Cobelli C, et al. SAAM II: simulation, analysis, and modeling software for tracer and pharmacokinetic studies. Metabolism 1998;47:484–92.

13. Gallo JM, Vicini P, Orlansky A, et al. Pharmacokinetic model-predicted anticancer drug concentrations in human tumors. Clin Cancer Res 2004;10:8048–58.

14. Zhou Q, Guo P, Kruh GD, et al. Predicting human tumor drug concentrations from a preclinical pharmacokinetic model of temozolomide brain disposition. Clin Cancer Res 2007;13:4271–9.

15. Jain RK, Ward-Hartley K. Tumor blood flow-characterization, modifications, and role in hyperthermia. IEEE Trans Sonics Ultrasonics 1984; SU-31:504–26.

16. Kim SG, Ackerman JJH. Quantitative determination of tumor blood flow and perfusion via deuterium nuclear magnetic resonance spectroscopy in mice. Cancer Res 1988;48:3449–53.

17. Gabrielsson J, Weiner D. Pharmacokinetic and pharmacodynamic data analysis: concepts and applications. Stockholm (Sweden): Swedish Pharmaceutical Press; 2000. p. 175–259.

18. Mager DE, Wyska E, Jusko WJ. Diversity of mechanism-based pharmacodynamic models. Drug Metab Dispos 2003;31:510–8.

19. Sirotnak FM, Zakowski MF, Miller VA, et al. Efficacy of cytotoxic agents against human tumor xenografts is markedly enhanced by coadministration of ZD1839 (Iressa), an inhibitor of EGFR tyrosine kinase. Clin Cancer Res 2000;6:4885–92.

20. Zamboni WC, D'Argenio DZ, Stewart CF, et al. Pharmacodynamic model of topotecan-induced time course of neutropenia. Clin Cancer Res 2003;7:2301–8.

21. Krzyzanski W, Jusko WJ. Integrated functions for four basic models of indirect pharmacodynamic response. J Pharm Sci 1998;87:67–72.

22. Caldwell GW, Ritchie DM, Masucci JA, et al. The new pre-preclinical paradigm: compound optimization in early and late phase drug discovery. Curr Top Med Chem 2001;1:353–66.

23. Engelman JA, Jänne PA, Mermel C, et al. ErbB-3 mediates phosphoinositide 3-kinase activity in gefitinib-sensitive non-small cell lung cancer cell lines. Proc Natl Acad Sci U S A 2005;102:3788–93.

24. Jain A, Tindell CA, Laux I, et al. Epithelial membrane protein-1 is a biomarker of gefitinib resistance. Proc Natl Acad Sci U S A 2005;102: 11858–63.

25. Paez JG, Jänne PA, Lee JC, et al. EGFR mutations in lung cancer: correlation with clinical response to gefitinib therapy. Science 2004;304: 1497–500.

26. Yoshida K, Yatabe Y, Park JY, et al. Prospective validation for prediction of gefitinib sensitivity by epidermal growth factor receptor gene mutation in patients with non-small cell lung cancer. J Thorac Oncol 2007; 2:22–8.

27. Omuro AM, Faivre S, Raymond E. Lessons learned in the development of targeted therapy for malignant gliomas. Mol Cancer Ther 2007;6: 1909–19.

28. Zhou Q, Guo P, Wang X, et al. Preclinical pharmacokinetic and pharmacodynamic evaluation of metronomic and conventional temozolomide dosing regimens. J Pharmacol Exp Ther 2007;321:265–75.

29. Luo FR, Yang Z, Dong H, et al. Prediction of active drug plasma concentrations achieved in cancer patients by pharmacodynamic biomarkers identified from the geo human colon carcinoma xenograft model. Clin Cancer Res 2005;11:5558–65.

30. Sharma A, Ebling WF, Jusko WJ. Precursor-dependent indirect pharmacodynamic response model for tolerance and rebound phenomena. J Pharm Sci 1998;87:1577–84.

31. Siegel RA. Investigation of a cellular pharmacodynamic model exhibiting sharp response sensitivity and tolerance. J Pharmacokinet Pharmacodyn 2007;34:87–101.

32. Simeoni M, Magni P, Cammia C, et al. Predictive pharmacokinetic-pharmacodynamic modeling of tumor growth kinetics in xenograft models after administration of anticancer agents. Cancer Res 2004;64: 1094–101.

Preclinical pharmacokinetic/pharmacodynamic models of gefitinib and the design of equivalent dosing regimens in EGFR wild-type and mutant tumor models

Shining Wang, Ping Guo, Xiaomin Wang, et al.

Updated version	Access the most recent version of this article at: http://mct.aacrjournals.org/content/7/2/407

Cited articles	This article cites 31 articles, 18 of which you can access for free at: http://mct.aacrjournals.org/content/7/2/407.full#ref-list-1
Citing articles	This article has been cited by 11 HighWire-hosted articles. Access the articles at: http://mct.aacrjournals.org/content/7/2/407.full#related-urls

E-mail alerts	Sign up to receive free email-alerts related to this article or journal.
Reprints and Subscriptions	To order reprints of this article or to subscribe to the journal, contact the AACR Publications Department at pubs@aacr.org.
Permissions	To request permission to re-use all or part of this article, use this link http://mct.aacrjournals.org/content/7/2/407. Click on "Request Permissions" which will take you to the Copyright Clearance Center's (CCC) Rightslink site.